Journal of
Materials Chemistry B

PAPER

View Article Online
View Journal

Cite this: DOI: 10.1039/c6tb02475k

A strategy for developing effective orally-delivered nanoparticles through modulation of the surface "hydrophilicity/hydrophobicity balance"†

Yi Cui,‡ Wei Shan,‡ Min Liu, Lei Wu and Yuan Huang*

Efficient oral delivery of macromolecules by nanoparticles is greatly limited by epithelial cells and the mucus layer that covers the surface of the intestinal epithelium. Worse still, to overcome both the mucus and epithelium barriers, opposite surface properties of the nanocarriers are required. Hydrophilic properties are necessary for mucus permeation, while hydrophobic ones are preferable for epithelium internalization. Thus, it is supposed that there must be a balance between the hydrophilicity and hydrophobicity of the surface of nanoparticles (NPs), which would provide NPs with a rapid mucus penetrating ability and satisfactory cellular uptake efficiency. In the current study, we have synthesized a series of copolymers (HPMA–FAs) composed of hydrophilic *N*-(2-hydroxypropyl) methacrylamide (HPMA) and four hydrophobic methacrylamido fatty acid ester (FA) analogues. By changing the amount of HPMA–octyl methacrylate (HPMA–C8) or applying different FAs on polymerization of the HPMA–FA copolymers for the NP formulation, we have formulated NPs with varied surface hydrophilicity/hydrophobicity properties. It was observed that the NPs coated with a 20% amount of the HPMA–C8 copolymers could result in a satisfactory mucus penetrating ability and cellular uptake efficiency, while the NPs coated with a 20% amount of the HPMA–cetyl methacrylate copolymer (NPs-C16 (20%)) presented the best results compared with the other HPMA–FA formulated NPs. The *in vivo* study showed that insulin-loaded NPs-C16 (20%) generated an obvious hypoglycemic effect, with a maximal 46% reduction of the blood glucose level. Moreover, no histopathology lesions or serum chemistry parameter changes were observed based on the *in vivo* toxicity test. Therefore, we hope that these results will provide a new perspective for the design of mucus-penetrating and epithelium-absorbed NPs for oral drug delivery systems.

Received 22nd September 2016,
Accepted 13th January 2017

DOI: 10.1039/c6tb02475k

rsc.li/materials-b

1. Introduction

Since the approval of recombinant insulin by the Food and Drug Administration (FDA), protein drugs have increased dramatically in number and have possessed a significant role in almost every field of medicine.[1–4] However, owing to their intrinsic vulnerable tertiary structures and high molecular mass, they can only be administered through parenteral routes currently, resulting in a high economic cost and poor patient compliance.[5–8]

The application of nanotechnology to medicine has enabled the development of nanocarriers,[9–12] which open a novel pathway for the oral application of protein drugs. The nanoparticles could protect the protein therapeutics from enzymatic degradation and modulate the release profile of the loaded drugs.[13–15] Unfortunately, due to the presence of a mucus layer and the underlying intestinal epithelial cells, the oral bioavailability of protein drugs is still limited.[16] Previous studies have reported that NPs with a hydrophobic or positively charged surface exhibit a strong affinity to epithelial cells and were demonstrated to improve the absorption of the loaded-drugs remarkably in *in vitro* studies.[17–19] Whereas once submitted to animal studies, the absorption efficiency was largely compromised.[20] This phenomenon was explained by the existence of a mucus layer, which could rapidly trap and remove foreign particles, especially those with cationic or hydrophobic surface properties.[21] To solve this problem, mucus penetrating particles were developed. NPs with hydrophilic and near neutral surface properties have been reported to favorably penetrate across mucus.[22] But the absorption efficiency of the drug-loaded NPs was subsequently limited because of the compromised affinity to cell membranes on fabricating a "mucus inert" surface.[23]

Key Laboratory of Drug Targeting and Drug Delivery System (Ministry of Education), West China School of Pharmacy, Sichuan University, No. 17, Block 3, Southern Renmin Road, Chengdu 610041, China. E-mail: huangyuan0@163.com; Fax: +86 2885501617; Tel: +86 2885501617

† Electronic supplementary information (ESI) available. See DOI: 10.1039/c6tb02475k

‡ Y. C. and W. S. contributed equally to this work.

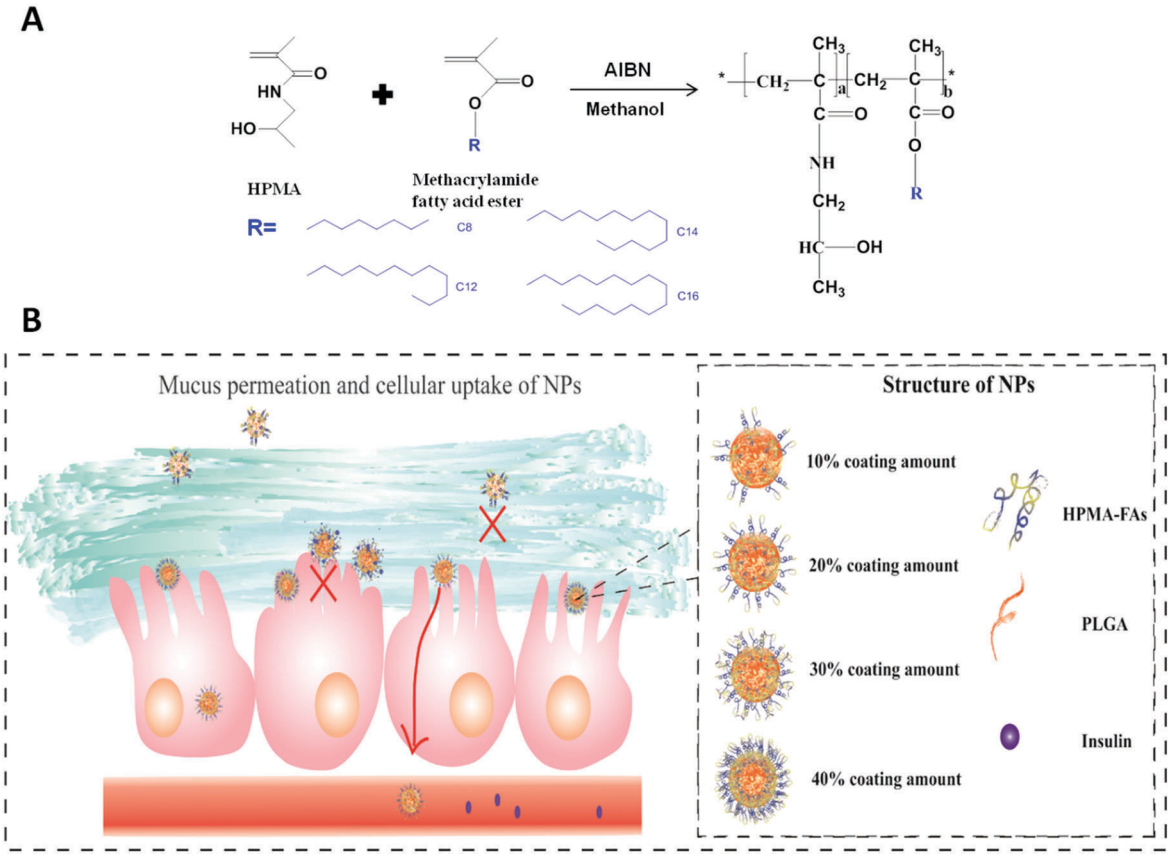

Fig. 1 (A) Chemical structure of the HPMA–FAs copolymers. The HPMA and FAs were polymerized randomly. "R" represents aliphatic methacrylates with different lengths of alkyl chains. (B) Schematic illustration of the process of permeation across the mucus layer and the cellular uptake of the NPs. As shown in the left image, both too little and too much coating would limit the bioavailability of the insulin incorporated in the NPs.

To achieve efficient absorption, NPs have to overcome the mucus layer and intestinal epithelial cells simultaneously. Hydrophilic nanocarriers are more favorable for mucus penetration, while hydrophobic ones are preferentially internalized by cells. Although nanocarriers for overcoming these two barriers require contradictory surface properties, is there a balance between the hydrophilicity and hydrophobicity of the particle surface that could result in a desirable mucus penetrating ability and cell membrane affinity?

N-(2-Hydroxypropyl) methacrylamide (HPMA) polymers have been explored as macromolecular carriers for chemotherapeutic agents for over thirty years because of their non-immunogenicity, non-toxicity, and biocompatibility.[24] Now, there are at least four HPMA-based therapeutics that have progressed into clinical trials.[25] Moreover, previous studies in our group have demonstrated that densely coating NPs with HPMA copolymers could significantly diminish the adhesive interactions of the NPs with the mucus layer and help them to rapidly penetrate through the mucus layer, thus this might be a promising coating material for mucus penetration.[26] In spite of the above positive results, the compromised affinity towards cells due to hydrophilicity was still a cause for concern.

In the current study, we have attempted to prepare HPMA polymer-based NPs that possess a satisfactory mucus permeability and cell absorption efficiency. HPMA–methacrylamido fatty acid ester copolymers (HPMA–FAs, Fig. 1A) composed of hydrophilic HPMA monomers and hydrophobic fatty acids were prepared. The HPMA–FAs could self-assemble on the surface of poly(lactic-*co*-glycolic acid) (PLGA)-based NPs (NPs-PLGA) to provide hydrophilic and near neutral surface properties. The NPs coated with different amounts of the HPMA–FA copolymers and the copolymers polymerized with different kinds of FAs exhibit various surface hydrophilicity/hydrophobicity properties. We then investigated their mucus permeability and cellular uptake efficiency (a schematic illustration of the NPs permeating across the mucus layer and transporting into the intracellular environment is shown in Fig. 1B). Moreover, the hypoglycemic effects and pharmacokinetics of the insulin-loaded NPs, and the tissue distribution and *in vivo* toxicity of the NPs were also evaluated.

2. Materials and methods

2.1. Materials

Poly(lactic-*co*-glycolic acid) (PLGA, 50/50, viscosity: 0.15–0.25 dL g^{-1}) with one carboxylic acid end group (PLGA–COOH) was purchased from Lactel absorbable polymers (Birmingham, US) and used without any further purification. *N*-Octyl methacrylate, lauryl

methacrylate, tetradecyl methacrylate and cetyl methacrylate were purchased from J&K Scientific Ltd (Beijing, China). Rose Bengal, chlorpromazine and lovastatin were all purchased from Sigma-Aldrich (St. Louis, MO). 1,1′-Dioctadecyl-3,3,3′,3′-tetramethylindocarbocyanine perchlorate (Dil) and Alamar Blue were purchased from Invitrogen (Carlsbad, CA, USA). Methyl-beta-cyclodextrin (M-β-CD) and rottlerin were purchased from Selleck Chemicals (Shanghai, China). Porcine insulin (27.9 IU mg^{-1}) was purchased from Wanbang Bio-Chemical Co. Ltd (Jiangsu, China). All other chemicals used were of analytical grade.

2.2. Cells and animals

In the current study, intestinal enterocytes like Caco-2 cells and goblet mucus-producing HT29-MTX-E12 (E12) cells were used. Cells were cultured using Dulbecco's Modified Eagle's Medium (DMEM; Invitrogen, USA), supplemented with 10% (v/v) fetal bovine serum (FBS, Gibco, USA), 1% (v/v) nonessential amino acid, 1% (v/v) L-glutamine, and 1% (v/v) penicillin and streptomycin (100 IU mL^{-1}) (all from Hyclone, UT, USA). The cells were cultivated in culture flasks maintained at 37 °C in an atmosphere of 5% CO_2 and 90% relative humidity. Male Sprague-Dawley rats (weighing 180–220 g) and ICR mice (weighing 18–22 g) were provided by Chengdu Dashuo Biological Technology (Chengdu, China). All the experiments were approved by the Institutional Animal Care and Use Committee of Sichuan University.

2.3. Synthesis and characterization of the HPMA–FAs derivatives

The monomers of *N*-(2-hydroxypropyl) methacrylamide (HPMA) were synthesized according to previous reports.[27,28] The polymerization of the HPMA monomers and methacrylamido fatty acid esters (FAs, including *N*-octyl methacrylate (C8), lauryl methacrylate (C12), tetradecyl methacrylate (C14), cetyl methacrylate (C16)) was performed *via* a radical solution copolymerization in methanol (azobisisobutyronitrile (AIBN), 2 wt%; monomer concentration, 12.5 wt%; molar ratio of HPMA/FA was 90 : 10, respectively). The copolymerization was carried out under nitrogen in sealed ampules at 50 °C for one day. The synthesized copolymers were named as HPMA–C8, HPMA–C12, HPMA–C14 and HPMA–C16. The HPMA copolymers were dialyzed against deionized water and then lyophilized. The HPMA monomers and polymers were characterized using ^1H nuclear magnetic resonance (NMR) spectroscopy (Bruker VANAN INOVA 400, Billerica, MA). The molecular weight (MW) and polydispersity index (PDI) of the HPMA polymers were determined using size exclusion chromatography with a Superose 200 10/300GL analytical column (Amersham Biosciences, NJ) using a Fast Protein Liquid Chromatography system (AKTA FPLC, Amersham Biosciences, NJ).

2.4. Preparation and characterization of the NPs

The NPs were prepared based on a self-assembled nanoprecipitation method.[29] Briefly, a desired amount of the HPMA–FAs and 2.0 mg PLGA were dissolved in 200 μL of dimethyl sulphoxide (DMSO). Then the DMSO solution was added dropwise into 2.0 mL of deionized water with magnetic stirring (1000 rpm). The prepared NPs were collected through centrifugation at 15 000*g* for 60 min. In order to prepare the fluorescence-labeled NPs, Dil (0.15% w/w), a hydrophobic fluorescent dye, was blended into the DMSO solution of PLGA and the HPMA–FA.[26] The nanoparticles were dispersed in phosphate buffer saline (PBS, 0.01 M, pH 7.3, 25 °C, I = 0.041) for zeta potential measurements with a Malvern Zetasize NanoZS90 (Malvern Instruments Ltd, UK). The zeta potential measurements were also performed in deionized water (pH 6.85, 25 °C). The morphology of the NPs was also examined using transmission electron microscopy (TEM, H-600, Hitachi, Japan). The prepared HPMA–FA NPs were termed accordingly as NPs-CX (*Y*%), where X represents the alkyl chain length of the FAs in the HPMA–FAs and Y is the percentage of the HPMA–FAs added (w/w, relative to PLGA).

To investigate the surface hydrophobicity of the NPs, Rose Bengal assays were performed.[30,31] Freshly prepared NPs (1 mL) were incubated with different concentrations (5–40 μg mL^{-1}) of the Rose Bengal dye (1 mL) for 3 h at room temperature, and then the test samples were centrifuged at 12 000*g* for 30 min. The free Rose Bengal dye in the supernatant was quantified using ultraviolet spectrophotometry, and the binding constant for binding of Rose Bengal (K) to the surface of the NPs was calculated according to the following equation:

$$\frac{r}{a} = KN - Kr$$

where r is the amount of Rose Bengal adsorbed per mg of nanoparticles (μg mg^{-1}); a is the equilibrium concentration of Rose Bengal (μg mL^{-1}); K is the binding constant (mL μg^{-1}); and N is the maximum amount bound (μg mg^{-1}).

To quantify the amount of HPMA–FAs coated on the surface, the NPs were purified through centrifuging at 15 000*g* for 60 min to remove the free HPMA–FAs. 0.036 mg samples for the XPS measurements were loaded onto a glass slide and dried under vacuum. Carbon, oxygen and nitrogen elemental spectra were obtained using X-ray photoelectron spectroscopy (XPS) (Siemens D5000 diffractometer). The area under the binding energies was calculated. The area under the binding energies for nitrogen was divided by that of the total element spectrum to calculate the percentage of nitrogen.

2.5. Mucin affinity analysis

To understand the interactions between the NPs and the mucus layer, the affinity of the NPs with mucin was investigated.[32] Freshly prepared Dil-labeled NPs were dispersed in a porcine mucin solution (5 mg mL^{-1}), then vortexed at 100 rpm and incubated for 30 min at 37 °C in a shaker (ZHWY-103B, Shanghai Zhicheng Ltd, China). The samples were centrifuged at 160*g* for 5 min and the precipitates were washed with phosphate buffer saline (PBS) twice. Then the fluorescence intensity of the precipitates was measured using a Varioskan Flash Multimode Reader (Thermo Fisher Scientific, USA).

2.6. Mucus penetrating ability of NPs

The ability for diffusion across the mucus layer of the NPs was evaluated using a Ussing chamber. Natural porcine intestinal

mucus was employed as the mucus model.[33] Briefly, 10 μL of mucus was placed uniformly between two polycarbonate membranes (Merck Millipore, 2.0 μm), like a sandwich complex, which was fixed in the Ussing chamber with a diffusion area of 0.49 cm^2. The donor compartments were filled with 3.0 mL of a Krebs-Ringer buffer containing the test sample prepared as Section 2.4 described. The acceptor compartments were filled with 3.0 mL of blank Krebs-Ringer buffer. The solutions on both sides were continuously aerated with air, and the device was maintained at 37 °C with a circulating water bath. At the determined time points, a sample aliquot (0.2 mL) was taken from the acceptor chamber and supplemented with equal volumes of pre-warmed blank Krebs-Ringer buffer. The amount of permeated NPs was determined using a Varioskan Flash Multimode Reader. The apparent permeation coefficient (Papp) was calculated using the following equation:

$$\mathrm{Papp} = \frac{\mathrm{d}Q}{\mathrm{d}t} \times \frac{1}{A \times C_0}$$

where $\mathrm{d}Q/\mathrm{d}t$ is the flux of Dil-labeled NPs from the donor side to the acceptor side; C_0 is the initial concentration of Dil-labeled NPs in the donor compartment, and A is the membrane area (cm^2).

2.7. Cytotoxicity of the NPs

The cytotoxicity of the NPs was evaluated with E12 cells using an Alamar Blue assay.[34] The cells were seeded into 96 well plates at a density of 1×10^4 cells per well and cultured for 48 h. Then the cells were incubated with 0.2 mL of the NPs for testing at different concentrations (100–600 μg mL^{-1}, based on the PLGA concentration). After incubation for 3 h, the NPs for testing were replaced with complete medium and the cells were incubated for a further 24 h. Then the cells were subjected to the Alamar Blue assay. The tests were performed in triplicate and cells incubated with Hank's balanced salt solution (HBSS) were employed as a negative control. Viability was expressed as a percentage of the negative control.

2.8. Intracellular uptake studies

For cellular uptake studies, the cells (Caco-2 cells and E12 cells) were incubated with Dil-labeled NPs at a PLGA concentration of 600 μg mL^{-1} for 3 h, which was followed by a thorough washing process to remove the attached samples. Then the cells were lysed, and the fluorescence intensity was measured using a Varioskan Flash Multimode Reader. The relative amount of uptake was corrected using the cell density, which was measured through the Alamar Blue assay. To further evaluate the influence of mucus on the NP uptake efficiency, the mucus layer of the E12 cells was removed with *N*-acetyl cysteine (NAC).[35] Then, the cells were incubated with Dil-labeled NPs. After 3 h of incubation, the pretreated and non-treated cells were subjected to a thorough washing process to remove the remaining mucus and the attached samples. The amount of NPs internalized into the cells was measured according to the process described above. The cell uptake was also investigated using confocal laser scanning microscopy (CLSM) (Leica, Germany). After 3 h of incubation, the cells were fixed with 4% paraformaldehyde, after being washed with phosphate buffered saline (PBS). Subsequently, the cells were stained with DAPI for nuclei identification.

For endocytosis mechanism studies, the E12 cells were pre-incubated with selective chemical inhibitors of the endocytic pathways (chlorpromazine 10 μM, lovastatin 10 μg mL^{-1}, methyl-beta-cyclodextrin (M-β-CD) 1 μg mL^{-1}, rottlerin 10 μM) for 30 min. Next, the cells were incubated with a NP suspension in the presence of the inhibitors. Lastly, the cells were lysed for fluorescence detection as described above.

2.9. Transepithelial transport studies

For the transepithelial transport study, a cell monolayer of the E12 cell line on a permeable membrane (Corning Costar Corp., Cambridge, MA, 3.0 μm) was used as an *in vitro* model to mimic the intestinal epithelial cell layer. The cells were cultured for 18–21 days and those cells with a transepithelial electrical resistance (TEER) exceeding 500 Ω cm^2 were used in the experiments. At the start of the experiment, the cells were washed and pre-equilibrated with Hank's balanced salt solution (HBSS, pH 7.4) for 30 min. Then the apical solution was replaced with NP suspensions for testing at a PLGA concentration of 600 μg mL^{-1} and the cells were incubated at 37 °C. To better mimic the gastrointestinal transit patterns of pharmaceutical dosage forms, the incubation was performed for 8 h.[36] During incubation, aliquots of the medium (200 μL) were withdrawn from the receiver chamber at different time intervals (1, 2, 4, 6 and 8 h) and 200 μL of fresh HBSS was added to the basolateral acceptor to maintain a constant volume. Then the permeated NPs were analyzed using a Varioskan Flash Multimode Reader. To assess the integrity of the cell monolayers, the TEER values were also measured during the experiment.

2.10. Insulin encapsulation and characterization

Insulin-loaded NPs were prepared by mixing 0.4 mg of porcine insulin, a desired amount of the HPMA–FAs and 2.0 mg of PLGA in 200 μL of DMSO; then the mixture was subjected to nanoprecipitation in 2.0 mL of deionized water. To evaluate the encapsulation efficiency (EE%) and drug loading efficiency (DL%) of the NPs, the insulin-loaded NPs were centrifuged at 15 000*g* for 60 min. The amount of insulin in the supernatant and the precipitate were both measured using a BCA assay kit (KeyGen Biotech Co. Ltd, Nanjing, China).[37] Then the EE% and DL% were calculated according to the follow equations:

$$\mathrm{EE}(\%) = \frac{\text{Amount of insulin in NPs}}{\text{Amount of insulin in NPs} + \text{Amount of insulin in supernatant}} \times 100$$

$$\mathrm{DL}(\%) = \frac{\text{Amount of insulin in NPs}}{\text{Total amount of NPs}} \times 100$$

2.11. *In vitro* drug release and enzymatic degradation

To investigate the insulin release profile, insulin-loaded NPs were added into 100 kDa dialysis units (Millipore) and then immersed in simulated gastric fluid (SGF, without pepsin, 37 °C) at pH 2.5. After 2 h, the medium was replaced by simulated intestinal fluid (SIF, without trypsin, 37 °C) at pH 6.8. At different time points, 200 μL of the test sample medium was withdrawn and the insulin that remained was measured.

To evaluate the enzymatic stability of the NPs, an insulin degradation study was carried out in SIF. Briefly, the samples for testing were added into the SIF and then incubated at 37 °C. At specific time points, aliquots (100 μL) of the medium were collected and the enzymatic interactions were terminated by adding 50 μL of an ice-cold HCl solution (0.1 M). Then, the remaining insulin was measured using a reverse-phase high performance liquid chromatography (HPLC) method (Agilent 1200 series, CA, USA).[26]

2.12. Hypoglycemic effect and pharmacokinetics

The hypoglycemic effect and pharmacokinetics of the NPs following oral administration were evaluated with diabetic rats. To induce the diabetic model, male Sprague Dawley rats (200 ± 20 g) were injected with streptozotocin (65 mg kg^{-1}) as previously described.[38] A rat that exhibited a fasting blood glucose level over 300 mg dL^{-1} after treatment for 5 days was considered to be diabetic.[39] The animals were fasted overnight but had free access to water prior to the experiments. They were randomly assigned to five groups (5 rats per group), followed by intragastric administration of an insulin solution (50 IU kg^{-1}) or insulin loaded-NPs (NPs-PLGA, NPs-C8 (20%), NPs-C16 (20%)) at a dose of 50 IU kg^{-1}, or subcutaneous injection (s.c.) of an insulin solution at of dose of 5 IU kg^{-1}. The blood glucose level was determined using a glucose meter (JPS-6, Yicheng Biotech. Co. Ltd Beijing, China). To investigate the pharmacokinetics of the insulin-loaded NPs, blood samples were collected from the tail veins and the plasma insulin levels were quantified using a porcine insulin ELISA kit (R&D system, Inc, MN, USA). The endogenic insulin value (before administration) was subtracted from the value obtained from the experiment for each rat. The pharmacological availability (PA%) and bioavailability (F%) relative to subcutaneous injection were analyzed using the following equations:

$$\mathrm{PA}(\%) = \frac{\mathrm{AAC}_{\mathrm{oral}} \times \mathrm{Dose}_{\mathrm{S.C.}}}{\mathrm{AAC}_{\mathrm{S.C.}} \times \mathrm{Dose}_{\mathrm{oral}}} \times 100$$

$$F(\%) = \frac{\mathrm{AUC}_{\mathrm{oral}} \times \mathrm{Dose}_{\mathrm{S.C.}}}{\mathrm{AUC}_{\mathrm{S.C.}} \times \mathrm{Dose}_{\mathrm{oral}}} \times 100$$

where AAC is the area above the curve of the blood glucose level and AUC is the area under the curve of the plasma insulin concentration.

2.13. Tissue distribution assay

To determine the tissue distribution of the NPs, the fluorescence-labeled NPs were orally administrated to ICR mice, which were fasted for 12 h before the experiment. The mice were treated with NPs at a dose of 40 mg kg^{-1} by oral gavage. At specific time intervals (3, 6, and 12 h),[40] the mice were killed and the heart, liver, spleen, lungs and kidneys were collected. Each sample collected was homogenized using a Precellys®24 lysis/homogenizer (Bertin Technologies, France) and then completely digested in NaOH solution. The test samples were centrifuged (15 000g) for 10 min, and the fluorescence intensity of the supernatant was measured. Mice orally administered with saline were used as a control, and the autofluorescence intensity of the tissue segment was subtracted from the test value for each mouse.

2.14. *In vivo* toxicity study

To evaluate the *in vivo* toxicity, the insulin-loaded NPs were orally administered to ICR mice at an insulin dose of 150 IU kg^{-1} for 7 consecutive days.[41] A group treated with saline was used as a control. The mice were fed with normal chow and water, and their general behaviour, toxicity symptoms and mortality were monitored before and after the administration every day. Then the mice were killed, and blood samples and tissues were collected. The blood samples were placed into tubes and left to stand for 1 h at 37 °C to separate serum. The obtained sera were analyzed using a clinical chemistry analyzer (Hitachi 7020). The obtained tissues were fixed, embedded, sectioned and then stained with hematoxylin and eosin (H&E) for the subsequent histopathologic analysis.

2.15. Statistical analysis

The statistical analyses of all the data were performed with a two-tailed Student's t-test (SPSS, Chicago, III). Experiments were performed in triplicate unless otherwise stated. All data are presented as the mean ± SD. Significant differences were defined as $^{*}P < 0.05$ and $^{\#}P < 0.001$.

3. Results and discussion

3.1. Synthesis and characterization of the HPMA–FA copolymers

Owing to the hydrophilicity and neutral charge density of HPMA polymers, using NPs coated with a HPMA polymer could significantly diminish the adhesive interactions with mucus and result in rapid mucus penetration. On the other hand, fatty acids with hydrophobic alkyl chains have been demonstrated to facilitate the cellular uptake of NPs.[42] To investigate the effect of fatty acids with different alkyl chain lengths on the mucus penetration and cellular uptake of NPs, a series of HPMA–FA copolymers (HPMA–C8, HPMA–C12, HPMA–C14 and HPMA–C16) were synthesized (Fig. 1A). All the HPMA–FAs presented an average molecular weight (MW) of ~65.0 kDa with a polydispersity of less than 1.3 (ESI,† Table S1). The HPMA–FAs were characterized using ^{1}H nuclear magnetic resonance spectroscopy (ESI,† Fig. S1–S6), and the fatty acid-grafting degree of the four copolymers was 10.5, 10.4, 10.6 and 10.4% (w/w), respectively.

3.2. Preparation and characterization of NPs with different amounts of HPMA–C8 copolymers

3.2.1. Preparation and characterization of the NPs. To prepare NPs with a different hydrophilicity/hydrophobicity,

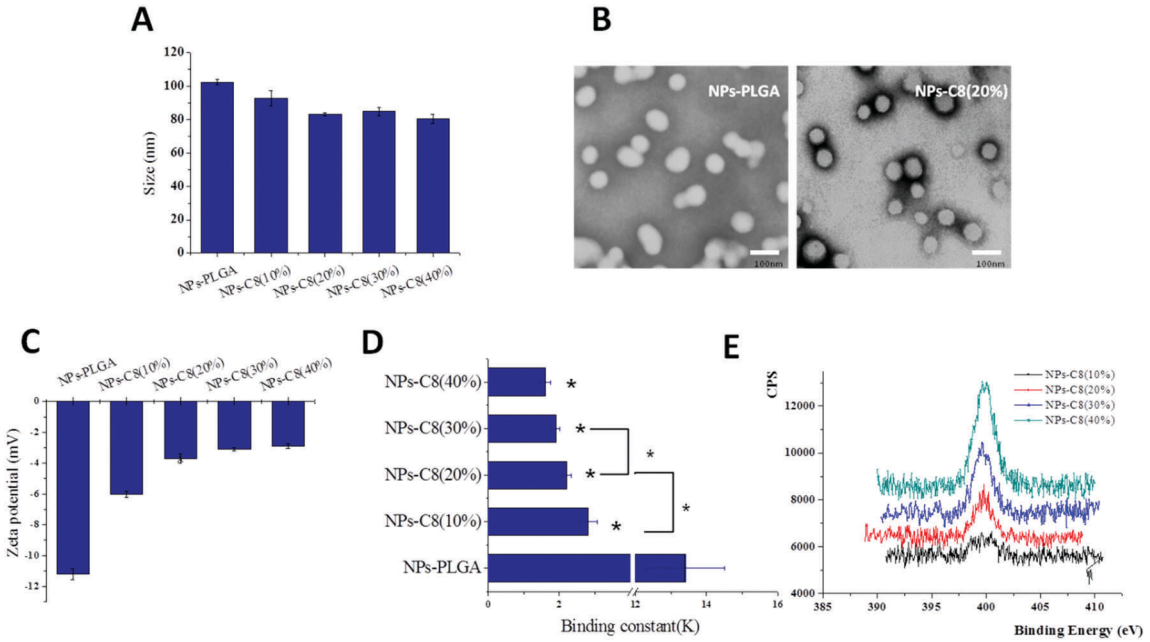

Fig. 2 (A) Size of the PLGA NPs coated with HPMA–C8. Prepared NPs were termed accordingly as NPs-C8 (*Y*%), where *Y* is the percentage of HPMA–C8 added (w/w, relative to PLGA). (B) TEM images of the NPs-PLGA and NPs-C8 (20%). (C) Zeta potential of the PLGA NPs coated with HPMA–C8. (D) The binding constant (*K*) for Rose Bengal was used as a measure of the surface hydrophobicity. Data are mean ± SD ($n = 3$), *$p < 0.05$. (E) Nitrogen element XPS spectrogram of the PLGA nanocomplex core coated with 10%, 20%, 30% and 40% HPMA–C8. The areas under the binding energies were calculated. The area increased as the amount of HPMA–C8 increased in the formulation.

various amounts of the HPMA–C8 copolymer (0, 10, 20, 30 and 40 wt% relative to PLGA) were mixed with PLGA, and then subjected to nanoprecipitation. As shown in Fig. 2A, the NPs-PLGA sample exhibited a size of 102.6 nm with a negative charge of −20.6 mV. However, after coating with the HPMA–C8 copolymer, the NPs showed a decrease in their size. This might be attributed to strong interactions between the HPMA–C8 and PLGA NPs, which would make the PLGA NPs more compact. Then the NPs-PLGA sample and the HPMA–C8 copolymer coated NPs were characterized using TEM images (Fig. 2B). All the NPs showed a well-defined spherical shape and a homogeneous size distribution around 80–100 nm in diameter, and the incorporation of HPMA–FAs did not cause morphological changes. As for the surface charges, coating HPMA–C8 copolymers on the surface of the PLGA NPs could shield their negative charges and the shielding efficiency varied with the coating amount of the HPMA–C8 copolymers. As shown in Fig. 2C, NPs coated with 40% HPMA–C8 relative to the PLGA (w/w) resulted in a nearly neutral surface charge of −2.9 mV (zeta potential measurement also performed in deionized water, see the ESI,† Table S2). When 0.8 mg of the HPMA–FA was added into the formulation, no particles were detected. What's more, the prepared NPs were collected through centrifugation at 15 000*g* for 60 min. This was a way to separate the free HPMA–FAs and nanoparticles. To some extent, all the formed nanomaterials are HPMA-coated PLGA nanoparticles.

To further quantify the amount of HPMA–FA coated on the surface, we chose to study the nitrogen atoms to present the content variation of the HPMA–FAs relative to the feed amount in the formulation using X-ray photoelectron spectroscopy (XPS). Specific element spectra were obtained including for carbon, oxygen, nitrogen. The area under the binding energies for nitrogen was divided by that of the total element spectra to calculate the percentage of nitrogen. As shown in Fig. 2E, the area under the binding energies for the nitrogen elements increased as more HPMA–C8 was added into the formulations. Based on the total element spectra, we calculated the nitrogen atom composition. Content values of about 1.12, 1.81, 2.34, and 3.09% were attributed to a PLGA nanocomplex core coated with 10%, 20%, 30% and 40% HPMA–C8, respectively (ESI,† Table S3). Therefore, these results indicate that the amount of HPMA–FA coated on the surface of the nanoparticles subsequently increased as an increasing amount was added into the formulation. Then the surface hydrophilicity/hydrophobicity properties of the NPs with varied amounts of HPMA–C8 copolymers were determined based on a Rose Bengal assay, and the hydrophobicity was characterized using the binding constant for Rose Bengal (*K*). As shown in Fig. 2D, the binding constant of NPs-PLGA was 13.4, while those of the four HPMA–C8 copolymer coated NPs were 2.8, 2.2, 1.9, 1.6, respectively. The binding constants of the NPs significantly decreased after coating with the HPMA–C8 copolymers, indicating an increased hydrophilicity of the HPMA–C8 coated NPs. Moreover, the hydrophilic surface properties of the HPMA–C8 copolymer coated NPs presented a coating amount-dependent manner.

3.2.2. Mucus diffusion ability of the NPs. To evaluate the mucus diffusion ability of the NPs, two different experiments were carried out. Mucin is the major component of mucus

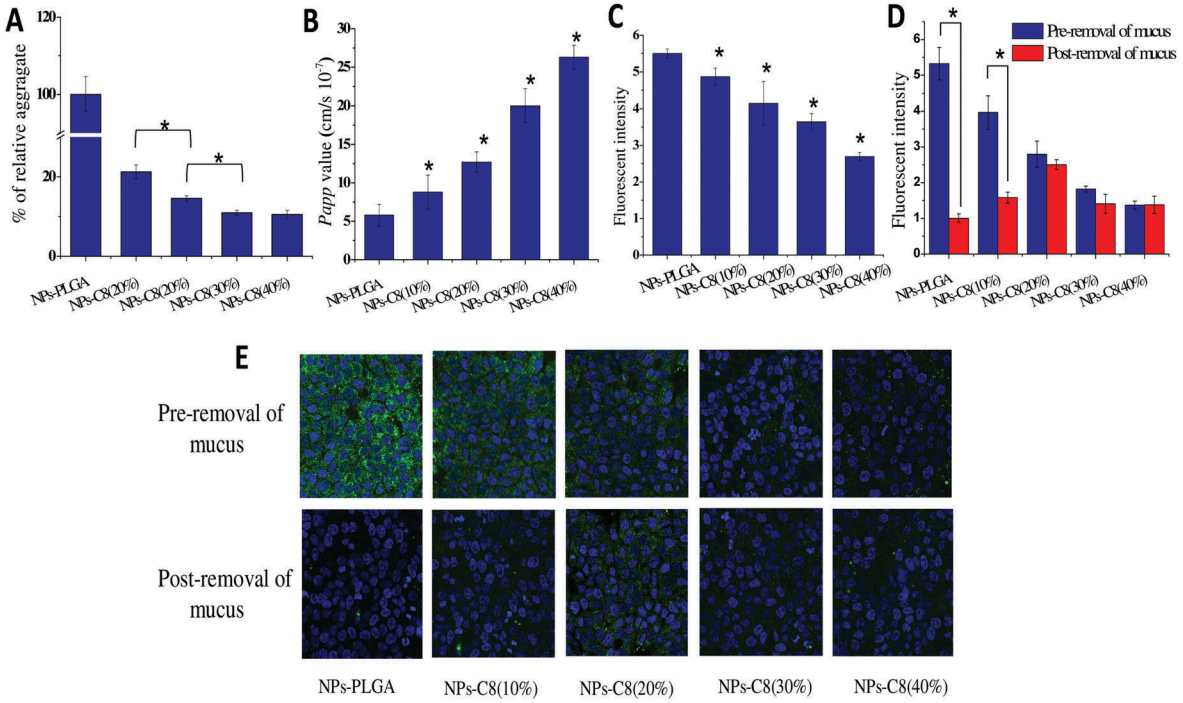

Fig. 3 (A) The fluorescence intensity for aggregates formed of mucin and the NPs. NPs-PLGA was used as a control and normalized to 100%. (B) Papp value for particle permeation across mucus from the donor and acceptor compartments of a Ussing chamber system. (C) Cellular uptake efficiency of the PLGA NPs coated with HPMA–C8 using Caco-2 cells. (D) Intracellular internalization of the particles using E12 cells with or without a pretreatment process to remove mucus. Data are mean ± SD (n = 3), *$p < 0.05$. (E) CLSM images of the intracellular internalization of the particles using E12 cells with or without a pretreatment process to remove mucus. Green fluorescence represents Dil-labeled NPs.

layers and could interact with NPs through hydrophobic and electrostatic interactions. Thus, we firstly investigated the formation of particle–mucin aggregates in a porcine mucin solution, which could provide some useful information for predicting the behavior of the nanoparticles when in contact with a mucus matrix. As shown in Fig. 3A, the NPs-PLGA sample exhibited a large amount of aggregates, formed with porcine mucin (as indicated by the fluorescence intensity), whereas after coating with the HPMA–C8 copolymers, the hydrophobic interactions with mucin remarkably diminished. The fluorescence intensity of the particle–mucin aggregates formed with NPs-C8 (10%) was 21.2 ± 1.74, which is 4.76-fold lower compared with NPs-PLGA. In addition, more HPMA–C8 coating led to a lesser amount of aggregates being formed with the porcine mucin. The fluorescence intensity of NPs-C8 (40%) was 10.53, which is 9.50-fold lower compared to NPs-PLGA. Then we investigated the diffusion of the NPs through a mucus layer using a Ussing chamber system. A porcine small intestinal mucus layer, which is similar to human intestinal mucus, was employed as a mucus model. As shown in Fig. 3B, the apparent permeability (Papp) value of NPs-PLGA was $(5.8 \pm 0.42) \times 10^{-7}$ cm s^{-1}. For HPMA–C8 copolymer coated NPs, the Papp values were much higher and increased along with the increasing amount of HPMA–C8. For example, the Papp value for NPs-C8 (10%) was $(8.8 \pm 2.21) \times 10^{-7}$ cm s^{-1}, whereas when the NPs were coated using a HPMA–C8 copolymer concentration of 40% (NPs-C8 (40%), the Papp value increased to $(26.3 \pm 1.56) \times 10^{-7}$ cm s^{-1}. These results indicate that coating HPMA copolymers on the surface of PLGA NPs could shield the hydrophobic regions and improve their mucus permeation ability. Moreover, different amounts of the HPMA–C8 copolymers endowed the NPs with varied hydrophilic properties and resulted in different mucus permeabilities, which showed a coating amount dependence.

3.2.3. Cellular uptake studies for the NPs. To evaluate the cellular uptake efficiency for the HPMA–C8 copolymer coated NPs, Caco-2 and E12 cell lines, representing enterocytes and mucus producing goblet cells, were employed as cell models. The cell viability with the NPs was measured using an Alamar Blue assay, and there was no statistically significant difference in the cell viability on using the tested NPs compared with the control group (ESI,† Fig. S7). Then, the cellular uptake of the NPs coated with different amounts of HPMA–C8 copolymers was investigated using Caco-2 cells. Owing to the strong affinity between PLGA NPs and the cell membrane *via* hydrophobic interactions, the NPs-PLGA sample presented the highest uptake efficiency (Fig. 3C) among all the samples tested. After shielding the hydrophobic regions with the HPMA–C8 copolymers, all the NPs showed a reduced cellular uptake compared with NPs-PLGA and also exhibited a coating amount-dependent manner. However, NP uptake by epithelial cells *in vivo* includes two processes: mucus penetration and epithelial cell uptake. Thus, the cellular uptake of the NPs was also investigated using mucus-producing cells. To investigate the influence of mucus on the uptake efficiency, a procedure was performed prior to the experiment to remove the cell mucus layer using NAC. Both

the cells pre-treated and not treated with NAC were incubated with the NPs for testing, and then washed thoroughly to remove any NPs that remained in the mucus. As shown in Fig. 3D, the cellular uptake results with E12 cells in the absence of a mucus layer were similar to those for Caco-2 cell lines, which again demonstrated that a hydrophilic surface could decrease the affinity of NPs to epithelial cells. However, the existence of mucus significantly changed the uptake behaviour of the NPs. As shown in Fig. 3D, NPs-PLGA exhibited the lowest uptake, while NPs coated with 20% of the HPMA–C8 copolymer led to the highest cellular uptake. It should be noted that with removal of the mucus the cellular uptake of NPs-PLGA and NPs-C8 (10%) was significantly depressed, whereas there were no statistically different changes for NPs-C8 (20%, 30% and 40%) compared to when the mucus existed. Although NPs-PLGA and NPs-C8 (10%) showed a higher uptake by Caco-2 cells, their strong hydrophobic interactions with mucus matrixes significantly limited their mucus penetrating ability. NPs-C8 (30%) and NPs-C8 (40%) presented excellent mucus penetrating abilities, but the strong surface hydrophilicity decreased their affinity for cell membranes and depressed their uptake efficiency. Only NPs-C8 (20%) showed an improved mucus penetrating ability and cellular internalization efficiency, which indicated a balance of the surface hydrophobicity and hydrophilicity. These results were further verified through CLSM investigation. Firstly, the cellular uptake was performed with pre-mucus removal cells. As shown in Fig. 3E, with an increased coating amount of HPMA–C8, the uptake of the NPs was coating amount-sensitive since the intracellular fluorescence intensity (green) of the nanoparticles became significantly reduced. However, the existence of mucus significantly changed the uptake behaviour of the NPs. As shown in Fig. 3E, the NPs coated with 20% of the HPMA–C8 copolymer exhibited the highest fluorescence intensity, while NPs-PLGA exhibited the lowest fluorescence intensity. The data were consistent with the previous results, further confirming that a balance between hydrophilicity and hydrophobicity existed on the surface of the nanoparticles.

3.3. Preparation and characterization of the NPs with different HPMA–FA copolymers

3.3.1. Preparation and characterization of the NPs. The above experiments have demonstrated that the NPs coated using 20% of the HPMA–C8 copolymer could achieve a balance of the hydrophilicity and hydrophobicity of the particle surface and result in a satisfactory mucus penetrating ability and cellular uptake efficiency. Methacrylamido fatty acid esters with different alkyl chain lengths could exhibit different interactions with the PLGA NPs, which might endow the NPs with varied hydrophilicities and hydrophobicities of the surface, and influence their mucus penetrating ability and cellular uptake efficiency. To investigate the influence of alkyl chain length, NPs coated with different HPMA–FA copolymers (including HPMA–C8, HPMA–C12, HPMA–C14 and HPMA–C16) were prepared and the content of the HPMA–FA copolymers was 20% (w/w) relative to PLGA. As shown in Fig. 4A, the sizes of the NPs were approximately 84.0 nm with a PDI less than 0.12, which indicates a narrow size distribution of the HPMA–FA coated NPs. As for the surface charge, no significant differences were observed among the HPMA–FA coated NPs. Then the surface hydrophobicity of the NPs was evaluated. As shown in Fig. 4C, the binding constants of the NPs varied with variation of the HPMA–FAs copolymer. For NPs-C16 (20%), the binding constant was 1.6, which is significantly smaller than that of NPs-C8 (20%) (2.2), indicating a stronger hydrophilic surface of NPs-C16 (20%). In the current study, the HPMA–FA copolymers were synthesized by polymerizing the HPMA monomers and methacrylamido fatty acid esters randomly. When the copolymers are coated on the surface of the NPs, some of the alkyl chains might stretch outside of the surface because of steric hindrance. Compared to the short-chain fatty acid, the palmitic acid with a 16-carbon moiety may exhibit stronger hydrophobic interactions and interact with the PLGA NPs more flexibly. Thus, a lesser amount of the fatty acid (palmitic acid) would stretch outside of the NPs, which would result in a smaller binding constant compared to the other NPs. Such a coating manner may also facilitate the mucus penetration ability of NPs-C16 (20%).

3.3.2. Mucus diffusion ability of the NPs. To investigate the mucus diffusion ability of the NPs prepared with different HPMA–FA copolymers, the particle–mucin affinity and porcine mucus permeability were also evaluated. Although NPs-C8 (20%) has been demonstrated to diminish the affinity with mucin proteins and facilitate the mucus permeation ability, an enhanced ability was observed for HPMA–FA coated NPs with a longer alkyl chain length. As shown in Fig. 4D, NPs-C16 (20%) formed the lowest amount of particle–mucin aggregates with a depression of 75% compared with NPs-C8 (20%). As for the porcine mucus permeability, the NPs-C16 (20%) sample showed a Papp value of $(17.6 \pm 1.72) \times 10^{-7}$ cm s^{-1}, which is 1.39-fold higher compared to NPs-C8 (20%) (Fig. 4E). These results were very consistent with the results of the Rose Bengal assay and indicated an improved mucus permeability with NPs-C16 (20%).

3.3.3. Cellular uptake and transepithelial transport of the NPs. To evaluate whether the enhanced mucus penetration ability would lead to a compromised cellular uptake efficiency, the cellular uptake of the NPs coated with different HPMA–FA copolymers was investigated using E12 cells. To our surprise, the NPs-C16 (20%) sample presented the highest cellular uptake efficiency among all the tested NPs (Fig. 4F), which was 1.48-fold higher compared to NPs-C8 (20%). This result indicates that coating the PLGA NPs with HPMA–C16 copolymers not only improved their mucus permeability, but also facilitated their cellular internalization. To further confirm the enhanced cell membrane affinity, a transepithelial transport study using NPs-PLGA, NPs-C8 (20%) and NPs-C16 (20%) was carried out with E12 cell monolayers. There were no significant changes in the transepithelial electrical resistance (TEER) values of the cell monolayers before and after incubation with the test samples, which indicated an integrity of the cell monolayers[43] (ESI,† Fig. S8A). We also used immunofluorescence staining to view the changes of the tight junctions (TJs) after treatment with the nanoparticles. As shown in the ESI,† Fig. S8B, a fluorescence signal from CLDN4 (a typical

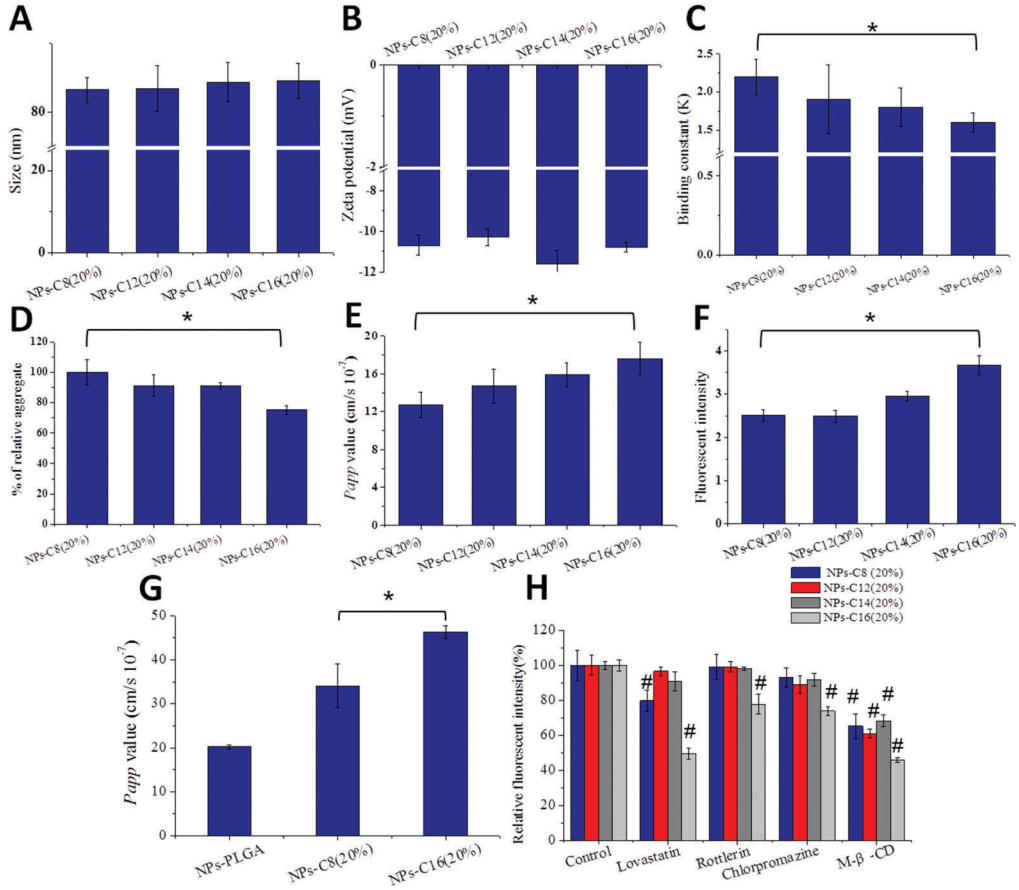

Fig. 4 Size (A) and zeta potential (B) of PLGA NPs coated with different HPMA–FA copolymers. (C) The binding constant (*K*) for Rose Bengal was used as a measure of the surface hydrophobicity. Data are mean ± SD (n = 3), *$p < 0.05$ *versus* each other. (D) The relative fluorescence intensity for aggregates formed of mucin and PLGA NPs coated with different HPMA–FA copolymers. The intensity of NPs-C8 (20%) was normalized to 100%. (E) Papp values for particle permeation across mucus from donor and acceptor compartments of the Ussing chamber system. (F) Intracellular internalization of the particles with E12 cells. Data are mean ± SD (n = 3), *$p < 0.05$ *versus* the NPs-C8 (20%) group. (G) Papp values of selected samples for an E12 monolayer with mucus in the transepithelial transport study. *$p < 0.05$ means a significant difference between NPs-C8 (20%) and NPs-C16 (20%). (H) Influence of endocytosis inhibitors (lovastatin, rottlerin, chlorpromazine and M-β-CD) on the exocytosis of the particles. Data are mean ± SD (n = 3), #$p < 0.001$ *versus* the control group.

TJ marker protein) was seen in the cytosol (Red),[44] which exhibited a continuous red ring appearance. These results demonstrate that the nanoparticles had no impact on the integrity of the TJs. Thus, all these results suggest that the NPs were transported through an intracellular pathway. As shown in Fig. 4G, the Papp values of the HPMA–FA coated NPs were obviously higher than for NPs-PLGA. Notably, the Papp value of NPs-C16 (20%) was $(40.2 \pm 1.39) \times 10^{-7}$ cm s^{-1}, which is significantly higher compared to NPs-C8 (20%).

The NPs-C16 (20%) nanoparticles with the highest mucus penetrating ability also exhibited the highest cell membrane affinity, which contradicts results obtained from the NPs prepared with different amounts of HPMA–C8 copolymer coating.

We speculated that the different degrees of uptake-facilitation of the fatty acids might be related to their endocytosis mechanisms. Thus, the cellular uptake mechanisms of the four HPMA–FA coated NPs were investigated using E12 cells. As shown in Fig. 4H, treatment with M-β-CD led to obvious inhibition for all the HPMA–FA coated NPs, which indicated the involvement of a lipid raft mediated endocytosis pathway. Lovastatin, a caveolae-mediated endocytosis pathway inhibitor, significantly reduced the cellular uptake of NPs-C8 (20%) and NPs-C16 (20%). The uptake was reduced by ~21% for NPs-C8 (20%) and 51% for NPs-C16 (20%). Rottlerin and chlorpromazine are non-specific inhibitors for macropinocytosis pathways and clathrin-mediated pathways, respectively. Interestingly, only NPs-C16 (20%) presented significant cellular uptake inhibition after treatment with rottlerin (22% reduction) and chlorpromazine (26% reduction), respectively. These results indicate that the NPs-C16 (20%) nanoparticles were involved in multiple pathways, including lipid raft and caveolae-mediated uptake, clathrin-dependent endocytosis and macropinocytosis, exhibiting a non-specificity of the endocytosis pathways, which may contribute to their high uptake.

3.4. Oral delivery of insulin to diabetic rats

3.4.1. Preparation and characterization of the insulin-loaded NPs. Owing to the rapid mucus penetration ability and satisfactory cellular uptake efficiency of NPs-C16 (20%)

Table 1 Physicochemical characteristics of the insulin-loaded NPs

Sample	Size (nm)	Zeta potential (mV)	EE%	DL%
NPs-PLGA	111.3 ± 2.51	−24.6 ± 0.43	55.5 ± 4.06	5.9 ± 0.39
NPs-C8 (20%)	97.6 ± 3.12	−12.1 ± 1.12	51.4 ± 1.40	5.7 ± 0.11
NPs-C16 (20%)	95.2 ± 1.75	−11.7 ± 1.35	53.4 ± 3.47	5.6 ± 0.31

in vitro, we subsequently employed insulin as a model drug and evaluated the hypoglycemic effect of insulin-loaded NPs-C16 (20%) *in vivo*. Insulin-loaded NPs-PLGA and NPs-C8 (20%) were chosen as controls. With NPs-C16 (20%), the insulin-loaded NPs showed a slight increase in their size (from 84.5 to 95.2 nm) after insulin loading, but no significant changes in their zeta potential (Table 1). The drug entrapment efficiency (EE%) and loading efficiency (DL%) were 53.4% and 5.6%, respectively. There was no significant difference between the two HPMA–FA coated NPs in terms of their size, surface charges, EE% and DL%. The insulin release profiles of NPs-C16 (20%) and NPs-PLGA were studied under simulated gastric and intestinal conditions to mimic their fate *in vivo* and the duration of the release in each medium was based on gastric and intestinal residence times. For the first 2 h, the NPs were exposed to simulated gastric fluids (SGF, without pepsin), and this was followed by 6 h in simulated intestinal fluids (SIF, without trypsin). As shown in Fig. 5A, a rapid insulin release of more than 60% was observed for NPs-PLGA, when the nanoparticles were subjected to SGF. As for NPs-C16 (20%), a sustained release occurred with less than 60% of the insulin released after 8 h of incubation. This result might be attributed to the coating of HPMA–FA on the surface of the PLGA NPs, and mediation of the insulin release profile. The stability of the insulin in the SIF was then evaluated. More than 20% of the insulin that was released from the nanoparticles can be accounted for by a simple diffusion mechanism.[45] Enteric coating would be an effective way to further enhance the bioavailability, as performed in our further studies.[46]

3.4.2. Hypoglycemic effects and pharmacokinetics of the insulin-loaded NPs. The hypoglycemic effects and plasma insulin concentration following oral administration of the insulin-loaded NPs were evaluated with diabetic rats.[47] In our previous study, the incorporation of insulin through our method and the use of DMSO had no apparent influence on the stability and activity of the insulin. Previously, we have already examined the bioactivity of insulin after a process of nanoparticle preparation.[32,48] As shown in Fig. 5C, the oral administration of a free insulin solution failed to reduce the blood glucose level, while the insulin-loaded NPs-C16 (20%) nanoparticles elicited an obvious hypoglycemic response with a maximal 46% reduction of the blood glucose level. In comparison, NPs-C8 (20%) only generated a mild hypoglycemic effect with

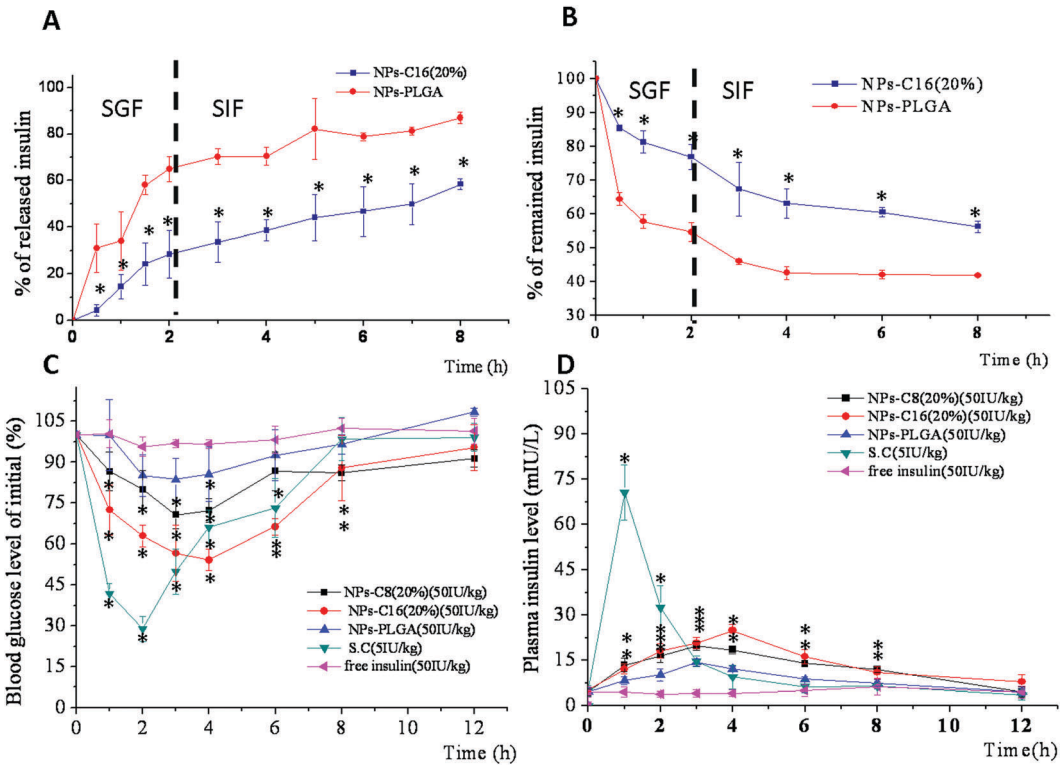

Fig. 5 (A) *In vitro* cumulative release profiles of insulin from the NPs in SIF over 8 h. (B) *In vitro* degradation profiles of insulin from the NPs over 8 h. All the experiments were performed at 37 °C and 100 rpm. Data are mean ± SD (n = 3), *$p < 0.05$ *versus* NPs-PLGA. (C) Variation of the blood glucose levels of diabetic rats after orally administering insulin loaded particles or an insulin solution at a dose of 50 IU kg^{-1}, or after subcutaneous injection of an insulin solution at 5 IU kg^{-1}. (D) Variation of the plasma insulin level of diabetic rats after orally administering insulin loaded particles or an insulin solution at a dose of 50 IU kg^{-1}, or after subcutaneous injection of an insulin solution at 5 IU kg^{-1}. Data are mean ± SD (n = 5), *$p < 0.05$ *versus* the oral free insulin group.

Table 2 Pharmacokinetic parameters of the different samples following administration

Sample	Administration route	Dose (IU kg^{-1})	T_{max} (h)	F (%)	PA (%)
Free insulin	Oral	50	—	0.89 ± 0.50	1.90 ± 0.56
NPs-PLGA	Oral	50	3	1.48 ± 0.42	2.96 ± 0.17
NPs-C8 (20%)	Oral	50	3	3.04 ± 0.28	5.34 ± 0.40
NPs-C16 (20%)	Oral	50	4	4.17 ± 0.31	6.53 ± 0.51
Insulin (s.c.)	s.c.	5	1	100	—

a maximal 30% reduction of the blood glucose level. The pharmacological availability (PA%) of the tested NPs relative to a subcutaneous injection of insulin was calculated. As shown in Table 2, NPs-C16 (20%) presented a PA value of 6.53%, which is 1.2-fold higher compared to NPs-C8 (20%) and 2.2-fold higher compared to NPs-PLGA. The plasma insulin concentration–time profiles are shown in Fig. 5D. The rats subcutaneously treated with a plain insulin solution at a dose of 5 IU kg^{-1} exhibited a rapid increase in the plasma insulin concentration, which reached a maximum at 1 h. Oral administration of the insulin-loaded NPs resulted in a slower rise in the insulin concentration, which reached a maximal insulin concentration nearly 4 h after treatment. Compared to NPs-PLGA and NPs-C8 (20%), NPs-C16 (20%) presented a significantly higher plasma insulin concentration at 4 h post-administration. The oral bioavailability (F%) of the insulin loaded in the NPs, relative to the subcutaneous injection, is shown in Table 2. All the insulin-loaded NPs exhibited improved oral bioavailability compared to the free insulin solution. NPs-C16 (20%) showed the highest oral bioavailability of 4.17%, which is 2.8-fold higher than for NPs-PLGA (1.48%).

3.5. Toxicity of the NPs

3.5.1. *In vivo* distribution of the NPs. To better understand the *in vivo* behaviour of the HPMA–FA copolymer coated NPs, the tissue distribution of NPs-C16 (20%) was investigated with ICR mice. The NPs were administered *via* gavage and the fluorescence intensity of the major organs was determined. The amount of NPs detected was expressed as a ratio of the fluorescence of each tissue relative to the sum of the fluorescence of all the tissues analyzed at 3 h after administration, and illustrated graphically in Fig. 6A. The NPs were detected in all the organs tested (heart, liver, spleen, lungs, and kidneys) and signals were measured even 12 h after treatment. From these results, it is evident that most of the NPs-C16 (20%) nanoparticles were distributed in the liver (49%), followed by the kidneys (27%), 3 h after administration. The highest accumulation amount of the NPs was in the liver as they pass through the portal veins following enterocyte-mediated absorption.[49] Hepatocytes are the most important targets for insulin to regulate the blood glucose level. Thus, the accumulation of NPs in the liver might be beneficial for delivery of

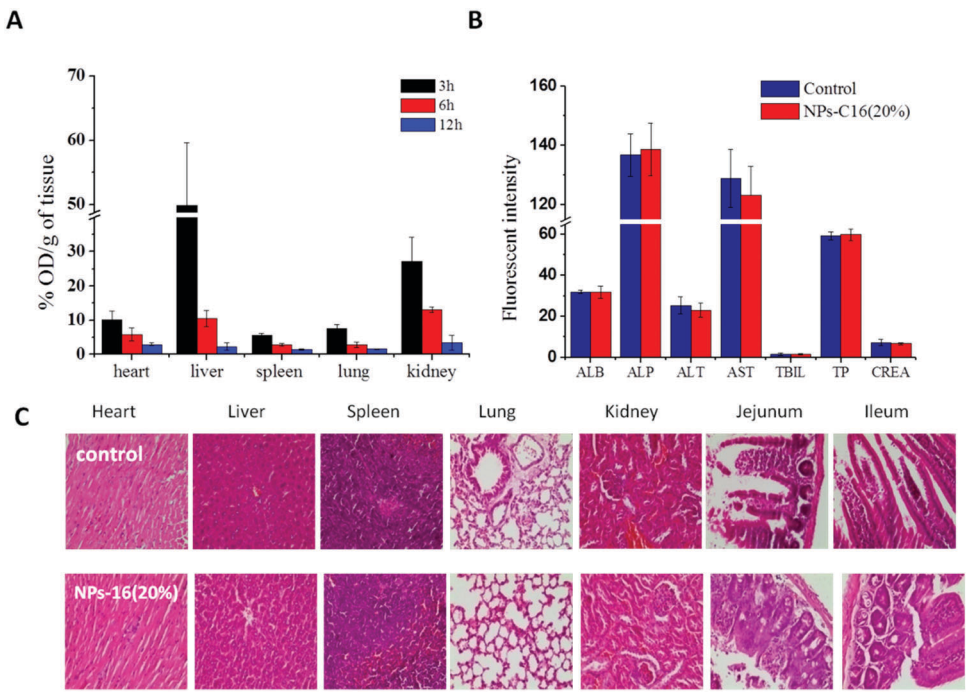

Fig. 6 (A) Biodistribution of Dil-labeled HPMA–C16 coated PLGA nanoparticles after oral administration. (B) Changes in the biochemical parameters for the serum of mice after administration of the NPs or saline. Data are mean ± SD (n = 5). (C) Morphological features of the various tissues (100×) from mice after 1 week of oral administration of NPs-C16 (20%) or saline.

insulin.[50] Due to most NPs being excreted *via* the kidneys, a relatively high distribution in the kidneys was also observed.[51]

3.5.2. Histopathology study and serum chemistry analysis. In order to investigate the toxicity of the NPs after oral administration, NPs-C16 (20%) was orally administered for 7 consecutive days, and then the histopathologic changes of the major organs (heart, liver, spleen, lungs, kidneys, jejunum and ileum) were checked. As shown in Fig. 6B, there were not any obvious histopathologic lesions for the mice treated with NPs-C16 (20%), compared to the mice treated with saline. In addition, owing to the large fraction of NPs detected in the liver and kidneys, a serum chemistry study was carried out to further evaluate the toxicity of the NPs with respect to liver function (ALB, ALP, ALT, AST, TBIL, and TP) and renal function (CREA). As shown in Fig. 6C, no obvious biological adverse effects were observed for all the listed clinical chemistry parameters, compared with the control group. All the results indicated that the HPMA–FA coated NPs could not cause any histopathologic lesions in mice or affect the functions of the liver and kidneys after oral administration.

4. Conclusion

The nanocarriers described herein were rationally designed to investigate the dilemma of requiring both mucus permeation and epithelial absorption to occur. We firstly changed the amount of HPMA–C8 copolymer in the NP formulation to prepare a series of NPs with various surface hydrophilicity/hydrophobicity properties. It was observed that the NPs coated with a 20% amount of the HPMA–C8 copolymer could result in a satisfactory mucus penetration ability and cellular uptake efficiency. Then, we applied HPMA–FA copolymers with four different FAs to alter the surface chemistry of the NPs. The NPs coated with a 20% amount of the HPMA–C16 copolymer presented the highest ability for mucus permeation and transepithelial absorption compared to the other NPs tested. An *in vivo* study showed that insulin-loaded NPs-C16 (20%) generated an obvious hypoglycemic effect with a maximal 46% reduction of the blood glucose level. No histopathology lesions or serum chemistry parameter changes were observed based on the *in vivo* toxicity test. Thus, understanding the role of the surface hydrophilicity/hydrophobicity of NPs will promote the development of efficient mucus-penetrating and epithelium-absorbed NPs for oral drug delivery systems.

Acknowledgements

We gratefully acknowledge financial support from the National Natural Science Foundation for Distinguished Young Scholars (81625023).

References

1 B. Leader, Q. J. Baca and D. E. Golan, *Nat. Rev. Drug Discovery*, 2008, **7**, 21–39.
2 A. K. Pavlou and J. M. Reichert, *Nat. Biotechnol.*, 2004, **22**, 1513–1519.
3 J. A. Davidson, L. C. Ramirez, P. Raskin and J. L. Selam, *Clin. Ther.*, 1991, **13**, 557–568.
4 T. Dingermann, *Biotechnol. J.*, 2008, **3**, 90–97.
5 R. I. Mahato, A. S. Narang, L. Thoma and D. D. Miller, *Crit. Rev. Ther. Drug Carrier Syst.*, 2003, **20**, 153–214.
6 R. B. Shah, F. Ahsan and M. A. Khan, *Crit. Rev. Ther. Drug Carrier Syst.*, 2002, **19**, 135–169.
7 M. D. DeMario and M. J. Ratain, *J. Clin. Oncol.*, 1998, **16**, 2557–2567.
8 S. S. Dychter, D. A. Gold, D. Carson and M. Haller, *J. Infusion. Nurs.*, 2012, **35**, 84–91.
9 F. Kesisoglou, S. Panmai and Y. Wu, *Adv. Drug Delivery Rev.*, 2007, **59**, 631–644.
10 M. Morishita and N. A. Peppas, *Drug Discovery Today*, 2006, **11**, 905–910.
11 P. Lundquist and P. Artursson, *Adv. Drug Delivery Rev.*, 2016, DOI: 10.1016/j.addr.2016.07.007.
12 R. H. Muller, C. Jacobs and O. Kayser, *Adv. Drug Delivery Rev.*, 2001, **47**, 3–19.
13 K. S. Soppimath, T. M. Aminabhavi, A. R. Kulkarni and W. E. Rudzinski, *J. Controlled Release*, 2001, **70**, 1–20.
14 C. Damge, P. Maincent and N. Ubrich, *J. Controlled Release*, 2007, **117**, 163–170.
15 S. D. Putney and P. A. Burke, *Nat. Biotechnol.*, 1998, **16**, 153–157.
16 Y. Jin, Y. Song, X. Zhu, D. Zhou, C. Chen, Z. Zhang and Y. Huang, *Biomaterials*, 2012, **33**, 1573–1582.
17 X. Wang, C. Zheng, Z. Wu, D. Teng, X. Zhang, Z. Wang and C. Li, *J. Biomed. Mater. Res., Part B*, 2009, **88**, 150–161.
18 D. A. Norris, N. Puri and P. J. Sinko, *Adv. Drug Delivery Rev.*, 1998, **34**, 135–154.
19 M. Morishita, T. Goto, N. A. Peppas, J. I. Joseph, M. C. Torjman, C. Munsick, K. Nakamura, T. Yamagata, K. Takayama and A. M. Lowman, *J. Controlled Release*, 2004, **97**, 115–124.
20 F. Y. Su, K. J. Lin, K. Sonaje, S. P. Wey, T. C. Yen, Y. C. Ho, N. Panda, E. Y. Chuang, B. Maiti and H. W. Sung, *Biomaterials*, 2012, **33**, 2801–2811.
21 F. Cui, K. Shi, L. Zhang, A. Tao and Y. Kawashima, *J. Controlled Release*, 2006, **114**, 242–250.
22 S. K. Lai, Y.-Y. Wang and J. Hanes, *Adv. Drug Delivery Rev.*, 2009, **61**, 158–171.
23 K. Maisel, L. Ensign, M. Reddy, R. Cone and J. Hanes, *J. Controlled Release*, 2015, **197**, 48–57.
24 R. Duncan, *Nat. Rev. Drug Discovery*, 2003, **2**, 347–360.
25 R. Duncan and M. J. Vicent, *Adv. Drug Delivery Rev.*, 2010, **62**, 272–282.
26 W. Shan, X. Zhu, M. Liu, L. Li, J. Zhong, W. Sun, Z. Zhang and Y. Huang, *ACS Nano*, 2015, **9**, 2345–2356.
27 K. Ulbrich, V. Šubr, J. Strohalm, D. Plocova, M. Jelınková and B. Říhová, *J. Controlled Release*, 2000, **64**, 63–79.
28 R. Duncan, H. C. Cable, J. B. Lloyd, P. Rejmanová and J. Kopeček, *Die Makromolekulare Chemie*, 1983, **184**, 1997–2008.
29 J. M. Barichello, M. Morishita, K. Takayama and T. Nagai, *Drug Dev. Ind. Pharm.*, 1999, **25**, 471–476.

30 S. Doktorovova, R. Shegokar, P. Martins-Lopes, A. Silva, C. Lopes, R. Müller and E. Souto, *Eur. J. Pharm. Sci.*, 2012, **45**, 606–612.
31 L. Brand, J. R. Gohlke and D. S. Rao, *Biochemistry*, 1967, **6**, 3510–3518.
32 X. Zhu, J. Wu, W. Shan, Z. Zhou, M. Liu and Y. Huang, *Adv. Funct. Mater.*, 2016, **26**, 2728–2738.
33 X. Zhu, J. Wu, W. Shan, W. Tao, L. Zhao, J. M. Lim, M. D'Ortenzio, R. Karnik, Y. Huang and J. Shi, *Angew. Chem., Int. Ed.*, 2016, **55**, 3309–3312.
34 M. McMillian, L. Li, J. Parker, L. Patel, Z. Zhong, J. Gunnett, W. Powers and M. Johnson, *Cell Biol. Toxicol.*, 2002, **18**, 157–173.
35 I. Behrens, A. I. V. Pena, M. J. Alonso and T. Kissel, *Pharm. Res.*, 2002, **19**, 1185–1193.
36 S. S. Davis, J. G. Hardy and J. W. Fara, *Gut*, 1986, **27**, 886–892.
37 R. A. Shimkunas, E. Robinson, R. Lam, S. Lu, X. Xu, X. Q. Zhang, H. Huang, E. Osawa and D. Ho, *Biomaterials*, 2009, **30**, 5720–5728.
38 B. Sarmento, S. Martins, D. Ferreira and E. B. Souto, *Int. J. Nanomed.*, 2007, **2**, 743–749.
39 G. Luippold, J. Bedenik, A. Voigt and R. Grempler, *PLoS One*, 2016, **11**, e0156346.
40 Z. Liu, W. Cai, L. He, N. Nakayama, K. Chen, X. Sun, X. Chen and H. Dai, *Nat. Nanotechnol.*, 2007, **2**, 47–52.
41 M. Liu, J. Zhang, X. Zhu, W. Shan, L. Li, J. Zhong, Z. Zhang and Y. Huang, *J. Controlled Release*, 2016, **222**, 67–77.
42 M. J. Cano-Cebrian, T. Zornoza, L. Granero and A. Polache, *Curr. Drug Delivery*, 2005, **2**, 9–22.
43 B. Srinivasan, A. R. Kolli, M. B. Esch, H. E. Abaci, M. L. Shuler and J. J. Hickman, *J. Lab. Autom.*, 2015, **20**, 107–126.
44 T. H. Yeh, L. W. Hsu, M. T. Tseng, P. L. Lee, K. Sonjae, Y. C. Ho and H. W. Sung, *Biomaterials*, 2011, **32**, 6164–6173.
45 P. Mukhopadhyay, S. Chakraborty, S. Bhattacharya, R. Mishra and P. P. Kundu, *Int. J. Biol. Macromol.*, 2015, **72**, 640–648.
46 D. Jiang, J. Zeng, Y. Zhu, G. Zhou, W. Deng, X. Xu and J. Yu, *Drug Dev. Ind. Pharm.*, 2016, **42**, 1174–1182.
47 B. Sarmento, S. Martins, D. Ferreira and E. B. Souto, *Int. J. Nanomed.*, 2007, **2**, 743.
48 E. M. Pridgen, F. Alexis, T. T. Kuo, E. Levy-Nissenbaum, R. Karnik, R. S. Blumberg, R. Langer and O. C. Farokhzad, *Sci. Transl. Med.*, 2013, **5**, 213ra167.
49 G. Mittal, D. K. Sahana, V. Bhardwaj and M. N. Ravi Kumar, *J. Controlled Release*, 2007, **119**, 77–85.
50 M. C. Chen, K. Sonaje, K. J. Chen and H. W. Sung, *Biomaterials*, 2011, **32**, 9826–9838.
51 P. A. Vasey, S. B. Kaye, R. Morrison, C. Twelves, P. Wilson, R. Duncan, A. H. Thomson, L. S. Murray, T. E. Hilditch, T. Murray, S. Burtles, D. Fraier, E. Frigerio and J. Cassidy, *Clin. Cancer Res.*, 1999, **5**, 83–94.